ZIRCONOCENE-CATALYZED OLEFIN POLYMERIZATION: MODELING OF CATALYST STABILITY, NONISOTHERMAL MODE OF OPERATION, AND SUPPORTED CATALYST CHARACTERIZATION

M. Atiqullah*, H. Hammawa, M. Faiz[1], M.N. Akhtar, M. Ahmed[2], J.H. Khan, A. Hassan

Center for Refining and Petrochemicals, The Research Institute
[1]Department of Physics
[2]Center for Applied Physical Sciences, The Research Institute
King Fahd University of Petroleum & Minerals, Dhahran 31261, Saudi Arabia

A.A. Abu Raqabah, A. Bin-Taleb, and M. Taftaf
R&T Complex, Saudi Basic Industries Corporation (SABIC)
P.O. Box 42503, Riyadh 11551, Saudi Arabia

الخلاصة :

تُوجز هذه الورقة مايلي: (أ) طريقة هندسية لحساب النشاط الحفزي وتحديد الثبات، (ب) تأثير البلمرة غير المتشابهة حرارياً، (ج) تعيين خواص حفازات الزيركوسين المثبتة غير المتجانسة باستخدام مطيافية الأشعة السينية للإلكترون الضوئي ومطيافية الأشعة السينية الناتجة عن تصادم البروتونات.

اعتمدت الطريقة الهندسية على نمذجة ذوبانية الإيثيلين في محلول البلمرة باستخدام متغيرات درجة الحرارة والضغط.

أما بخصوص البلمرة غير المتشابهة حرارياً؛ فإن تغيير معدل الخلط من أسلوب التحكم - النفاذي إلى غير النفاذي بدون انتقال المقاومة للغاز - السائل، أدى إلى زيادة الناتج الحراري للتفاعل وزمن التفاعل الحفزي. ولقد أظهرت النتائج أن تركيبة البوليمر وتوزيعها والمحلول الناتج من حفاز الزيركوسين يتأثر بعوامل الخلط والتغييرات الحرارية. ولقد أدى إضافة الهيكسين - ١ للتفاعل إلى خفض معدل الوزن الجزيئي والكثافة وأيضاً زيادة النشاط الحفزي ودرجة ذوبان وَتَبلُّر المحلول، وأدّى التغير الحراري إلى توسيع مؤشر التوزيع الجزيئي للبوليمر.

أظهرت نتائج مطيافية الأشعة السينية (XPS) أن تثبيت حفاز الزيركوسين على السيليكا في محلول (MAO) أدّى إلى نوعين من الأيونات الموجبة بغض النظر عن طرق التثبيت. ويعتقد أن الأيون الأول على هيئة ثنائي السيليكا وحفاز الزيركوسين، أما الأيون الثاني فهو محصور في مركب (MAO) وفي غياب مركب (MAO) فيتم الحصول على أيون إيجابي واحد.

وأظهرت النتائج أن العناصر القليلة التركيز تظهر على شكل شوائب تؤدي إلى تسمم الحفاز المثبت وذلك بواسطة مطيافية الأشعة السينية (PIXE).

*Corresponding author: e-mail: matiq@kfupm.edu.sa

ABSTRACT

This paper summarizes (*a*) an engineering approach to calculation of catalytic activity and stability profile, (*b*) influence of nonisothermal polymerization mode, (*c*) and characterization of supported zirconocene catalysts by X-ray photoelectron spectroscopy (XPS) and micro-proton induced X-ray spectroscopy (micro-PIXE).

The engineering approach is based on modeling the solubility of ethylene in the polymerization diluent as a function of temperature and pressure.

Under the nonisothermal mode of polymerization, a change in stirring level from diffusion-controlled regime to nondiffusion-controlled, external gas–liquid mass transfer resistance-free one, increased the reaction exotherm and the run time-average catalytic activity. The copolymer composition distribution and soluble fraction generated by $Et(Ind)_2ZrCl_2$ was sensitive to mixing conditions and thermal perturbations. Incorporation of 1-hexene significantly decreased the average molecular weights and density but increased the average catalyst activity, the peak melting temperatures and the weight- and number-average solution crystallization temperatures. Thermal perturbations broadened the polydispersity index.

XPS results showed that heterogenization of $Et(Ind)_2ZrCl_2$ on silica in the presence of MAO generated two types of zirconocenium cations (Cations 1and 2), irrespective of the heterogenization procedures. Cation 1 is presumed to be in the form of an ion-pair $[SiO]^-[Et(Ind)_2ZrCl]^+$ while Cation 2, a trapped multi-coordinated crown complex of MAO. In absence of MAO, only Cation 1 is formed.

Trace element impurities such as K, Ca, Ti, Fe, Ni, Cu, and Zn detected by micro-PIXE may be the potential sources of poisoning the heterogenized catalyst.

ZIRCONOCENE-CATALYZED OLEFIN POLYMERIZATION: MODELING OF CATALYST STABILITY, NONISOTHERMAL MODE OF OPERATION, AND SUPPORTED CATALYST CHARACTERIZATION

INTRODUCTION

The versatile superiorities of metallocene catalysts over the current Ziegler-Natta ones are already established [1]. Research efforts have recently started to affect the existing olefin polymerization technology on a commercial level. Metallocene-based polyolefins that are on the market have been recently reported in the literature [2]. Several factors are operating to advance this recent trend, mainly in the applied research area. These include the structural modification of metallocenes, the associated cocatalysts, and supports, and application of process development and/or retrofitting concepts, *etc.*

A comprehensive literature review [1] completed by the Center for Refining and Petrochemicals of the King Fahd University of Petroleum and Minerals (KFUPM) for Saudi Basic Industries Corporation (SABIC) shows the following. The current and future demands in metallocene-catalyzed olefin polymerization concerns how to (*a*) heterogenize commercially available metallocenes of simpler structures and modified cocatalysts and supports and (*b*) retrofit and/or develop a cost- and energy-effective polymerization process. These demands are shifting the research trend from fundamental to applied, particularly in the development of novel metallocene heterogenization and polymerization processes. The resin particulate morphology varies with the variation of the heterogenization and polymerization processes.

The overall catalyst development work requires elaborate laboratory-scale, solution and slurry polymerization trials. The common features in either case are:

(*i*) The monomer dissolves in the solvent or diluent; and

(*ii*) The polymerization depends on temperature, monomer solubility, reactor mixing conditions [3–7], *etc.*

The above literature review [1] also shows that the catalyst activity values have been measured from experiments that mostly ignored mass transfer limitations and micromixing effects. Hence, experimental reproducibility remains a question. Varying units such as *(g polyolefin formed)/{(mol or g metallocene) (hr)}, (g polyolefin formed)/{(mol or g metallocene) (hr) (psi of monomer pressure)}, etc.* have been used to report the values on an average scale. Consequently, the reported values cannot be consistently compared.

The dynamic stability of the metallocene catalyst systems has not been adequately addressed. Therefore, the effect of the resulting catalyst on the reactor start-up procedure cannot be evaluated. Experiments have been mostly conducted for one hour. For highly active systems, experimental limitations in certain cases even did not permit that [1].

The above remarks hold particularly to the results reported in patents. Hence, a consistent engineering approach that involves the simultaneous measurement of catalyst activity and stability should be developed.

The published results of metallocene-catalyzed, isothermal olefin polymerization has several limitations. It does not illustrate the influence of mixing, reaction exotherm, kinetic stability of the experimental metallocenes, and thermal perturbations on the catalytic activity, polymerization performance, and the properties of the resulting polymers. The mixing effects on general polymerization reactions and on the properties of the resulting polymers has already been documented to be significant in the literature [3–7].

In a typical polymerization, temperature varies during start-up, thermal runaway, *etc.* Consequently, the polymerization environment differs from that conducted isothermally even when varying the polymerization run temperature. Therefore, a facile experimental methodology should be developed that can evaluate the influence of the above process development factors. Uncontrolled, nonisothermal polymerization shows promise. Under a set of given experimental conditions, the measured reaction exotherm profile reflects the rate of generation of the catalytically active metallocenium ion. Moreover, the nonisothermal polymerization approximates a limiting case of thermal perturbations.

Several problems are outstanding in metallocene heterogenization. The catalytic activity of heterogenized metallocenes drastically decreases. The catalyst precursors leach off the support. The molecular weight distribution

broadens while the average molecular weight and melting point of the resulting polyolefins increase. The growing industrial success of metallocene catalysts depends on overcoming these problems. We would like to partially address these problems by studying the heterogenized solid-state electronic environment.

The literature does not show any work on the characterization of heterogenized metallocenes using X-ray photoelectron spectroscopy (XPS). Consequently, the electronic environment resulting from heterogenization and the interaction between the metallocenes, the methylalumoxane (MAO) cocatalyst, and the support remains unexplored. Moreover, such a study will help us understand (*a*) why the catalytic activity decreases; (*b*) how the polymer chain propagates, transfers, and terminates; and (*c*) how the stereoregulation occurs, particularly in the presence of the solid support. This prompted us to characterize the C_2 symmetric, chiral $Et(Ind)_2ZrCl_2$, heterogenized in the presence of MAO on silica, using XPS. Note that $Et(Ind)_2ZrCl_2$ homopolymerizes ethylene and propylene as well as copolymerizes them with α-olefins [1].

Therefore, based on the technical discussion between the Research Institute (of KFUPM) and SABIC research teams, the following metallocene-related technical issues were identified:

- Development of an engineering approach to measure catalyst activity and stability;
- Potentials of nonisothermal polymerization and the associated influence of mixing; and
- Investigation of heterogenization mass transport process and the resulting solid-state surface chemistry.

AN ENGINEERING APPROACH TO CALCULATE CATALYTIC ACTIVITY AND STABILITY

We first modeled the solubility of olefin in toluene, the most widely used solvent/diluent [1], as a function of temperature and pressure, then compared the model-predicted solubility values with the experimental data. The output of this model and the time-dependent olefin feed rate was used to develop the above engineering approach. We assumed the following:

(*i*) The polymer-free mixture approximates the pure solvent/diluent [8–10].

(*ii*) The vapor and liquid phases are in thermodynamic equilibrium. Hence, the fugacity in the corresponding phases is equal [11–18].

(*iii*) The low catalyst and cocatalyst concentrations do not affect the olefin solubility.

(*iv*) The olefin solubility in the polyolefin-free solvent/diluent does not change assuming that the stirrer speed is high enough to overcome the heat and mass transfer limitations.

(*v*) The application of a cubic equation of state holds because polyolefin does not dissolve in the diluent at the usually reported polymerization temperatures.

Based on the above assumptions, the solubility of ethylene and propylene in the polymerization diluent (toluene) can be calculated as a function of temperature and pressure. The detailed mathematical formulation appears elsewhere [17, 18]. What follows describes how the calculated olefin solubility can be incorporated to calculate the polymerization rate, activity, and stability profile.

Consider that the polymerization occurs in a semi-batch reactor. To calculate the stability and run time-dependent average activity of the catalytic system, we make a material balance of the monomer (olefin) M on the polymer-free solvent/diluent. This gives the following equation.

$$\dot{F}_M(t) - r_p(t)V^L = \frac{d(V^L c_M)}{dt} \tag{1}$$

where $\dot{F}_M(t)$ is the monomer molar flow rate; $r_P(t)$ is the monomer polymerization rate; $V^L c_M$ the total dissolved monomer in the polymerizing diluent, is constant [see assumption(s)]. Therefore,

$$r_p(t) = \dot{F}_M(t)/V^L . \tag{2}$$

Equation 2, normalized with respect to the catalyst amount M_{cat} and the monomer solubility c_M, appears as:

$$\hat{r}_P(t) = \dot{F}_M(t)/(M_{cat}c_M) . \tag{3}$$

Note that the above equation gives the normalized instantaneous catalytic activity $\hat{r}_P(t)$ in terms of (mass of polymer formed)/{(mole of cat)(molar concentration of monomer)(time)}. $\hat{r}_P(t)$ incorporates the combined influence of temperature and pressure because c_M is affected by these factors. Plotting this instantaneous activity as a function of time shows the stability of the catalyst system.

The average catalytic activity corresponding to a given polymerization run time t_R is given by:

$$\bar{r}_P(t_R) = \frac{1}{t_R}\int_0^{t_R} \dot{F}_M(t)/(M_{cat}c_M)dt \,. \tag{4}$$

EXPERIMENTAL

Polymerization

Ethylene (99.95% pure) was homopolymerized as well as copolymerized with 1-hexene in a one-liter Parr reactor using MAO-preactivated $Et(Ind)_2ZrCl_2$ and dried toluene. Table 1 summarizes the overall polymerization conditions in the foot note. Ethylene was fed to the reactor for one hour in a semi-batch mode. This semi-batch operation replenished the consumed amount thereby maintaining a constant polymerization pressure (see Table 1). The resulting polymerization temperature was monitored as a function of reaction time. Remaining polymerization details are available elsewhere [19].

The polymerization was quenched by stopping the ethylene supply, venting the reactor and adding 5 to 7 ml of methanol acidified with 2.5 vol% HCl. The filtered polymer was washed and then dried for 10 to 12 hours under vacuum to a constant weight.

The polymerization runs were conducted at 450 and 900 rpm which correspond to two distinct mixing regimes: diffusion-controlled and nondiffusion-controlled, gas–liquid mass transfer resistance-free, respectively [7–9].

The resulting polymers were characterized in terms of thermal properties, weight- and number-average solution crystallization temperatures, average copolymer composition, density, weight- and number-average molecular weights and polymer molecular weight distributions, commonly expressed as polydispersity index (PDI), using methods that have been detailed elsewhere [19].

Catalyst Preparation and Characterization

Davison Silica 955 having a surface area of 300 m^2/g, average pore volume of 1.65 cm^3/g, and pore size of 220 Å was partially dehydroxylated in vacuo by heating at 275°C for 24 hr in a Büchi furnace, then was cooled to room temperature and stored under argon. $Et(Ind)_2ZrCl_2$ and MAO (10% by wt. in toluene) were procured from Witco, Germany. Toluene from Aldrich was dried by refluxing in Na/Benzophenone. All manipulations were carried out in an inert atmosphere of argon using the Schlenk technique.

Table 1. Polymerization Activity of $Et(Ind)_2ZrCl_2$ and the Thermal Characteristics of the Resulting Polymers.

Polymerization run	Level of stirring (rpm)	Peak reaction exotherm (°C)	Catalyst activity (kg PE/[mol Zr h])	Peak melting point (°C)	Density (g/cm^3)	T_w (°C)	T_n (°C)	T_w:T_n
Homopolymer	950	41	4201.6	134.4	0.962	81.7	82.2	0.994
Copolymer 1	450	40	7044.7	129.8	0.918	68.0	61.1	1.113
Copolymer 2	950	56	7128.9	126.1	0.922	59.2	53.8	1.101

Ethylene feed pressure: 31 ± 1 psi; temperature: 50 ± 1°C; catalyst concentration: ~23.5 µmol Zr/l solvent; initial 1-hexene concentration: ~240.0 µmol/l; cocatalyst to catalyst ratio (Al:Zr molar ratio): ~2,383.

T_w and T_n are weight-average and number-average solution crystallization temperatures, respectively.

$Et(Ind)_2ZrCl_2$ was heterogenized on the above partially dehydroxylated silica using the following preparatory methods:

- Method 1: Adsorption of the zirconocene first, then treatment of the supported zirconocene with MAO;
- Method 2: Adsorption of MAO on silica first, then addition of the zirconocene in a second step; and
- Method 3: Addition of MAO-pretreated zirconocene to silica.

The details of the above heterogenization methods appear elsewhere [20].

XPS Experiments

The XPS spectra of the heterogenized catalysts were obtained using a VG-ESCALAB-MKII photoelectron spectrometer. The spectrometer energy was calibrated by fixing Cu $2p_{3/2}$ and Au $4f_{7/2}$ peaks at binding energies 932.67 and 83.98 eV, respectively [21].

The catalyst samples were first embedded in an indium foil placed in a metal sample holder. Then they were introduced into the air-lock chamber while the analysis chamber maintained a base pressure of 10^{-10} mbar.

From the air-lock chamber, the samples were subsequently transferred to the analysis chamber. Unmonochromated, 1486.6 eV Al $K\alpha$ photons were used at 130 W as the incident beam. The kinetic energy of the photoelectrons was analyzed using a multi-channeltron hemispherical energy analyzer with pass energy set at 20 eV in a fixed analyzer transmission (FAT) mode. Silica is an inert support; therefore, its Si 2p level binding energy, which is 103.4 eV [21], was used as the reference as well as to correct the energy shift. Data acquisition and analysis were performed by the VG-Eclipse software package.

Micro-PIXE Measurements

The heterogenized catalyst samples were pelletized and scanned using the micro-PIXE facility on the 3 MV Tandetron accelerator at the Center for Applied Physical Sciences of the Research Institute [22, 23], King Fahd University of Petroleum & Minerals, Dhahran.

X-Rays from the target, produced by the proton microbeam, were detected by the Si(Li) detector placed at an angle of 135° with respect to the incident beam direction. Signals from the detector were amplified, and processed by the CERN's VALET-Plus data acquisition and experiment control software [24] based on a VME computer interfaced through a PC. The data acquisition system produced simultaneously an X-ray energy spectrum and several two-dimensional elemental distribution maps from the scanned area on the target. The energy spectrum identified the elements present in the sample and the distribution maps showed the spatial concentration profiles of the elements.

In the present measurements, a pellet area of about 500 μm × 500 μm, divided into 64 × 64 pixels, was scanned at a time using a 2.5 MeV proton microbeam of about 5 μm resolution. The resulting elemental distribution maps were analyzed and printed on a grey concentration scale using the Kmax software [25]. The elemental spectra were analyzed using the PIXE quantitative analysis software GUPIX [26] to obtain the relative elemental concentrations.

RESULTS AND DISCUSSION

Polymerization Rate Model

Figures 1 and 2 compare the model-predicted solubility of ethylene and propylene as a function of temperature at various pressures with the corresponding experimental values, respectively. The computational scheme and the required thermodynamic properties are described in Reference [17]. For ethylene, the model prediction at 1, 5, and 10 atm well matches the experimental data obtained from the literature [27–31]. For propylene at 1 and 7 atm, the agreement is well whereas at 5 atm, the comparison with the experimental data deviates a little. So far as the influence of temperature is concerned, the result appears to deviate around 50°C and beyond.

Figure 3 plots the normalized polymerization rate, calculated following the current engineering approach, for the Cp_2ZrCl_2/MAO catalyst system. The ethylene volumetric input flow rate (cm^3/min) and the associated polymerization conditions were taken from Reference [32].

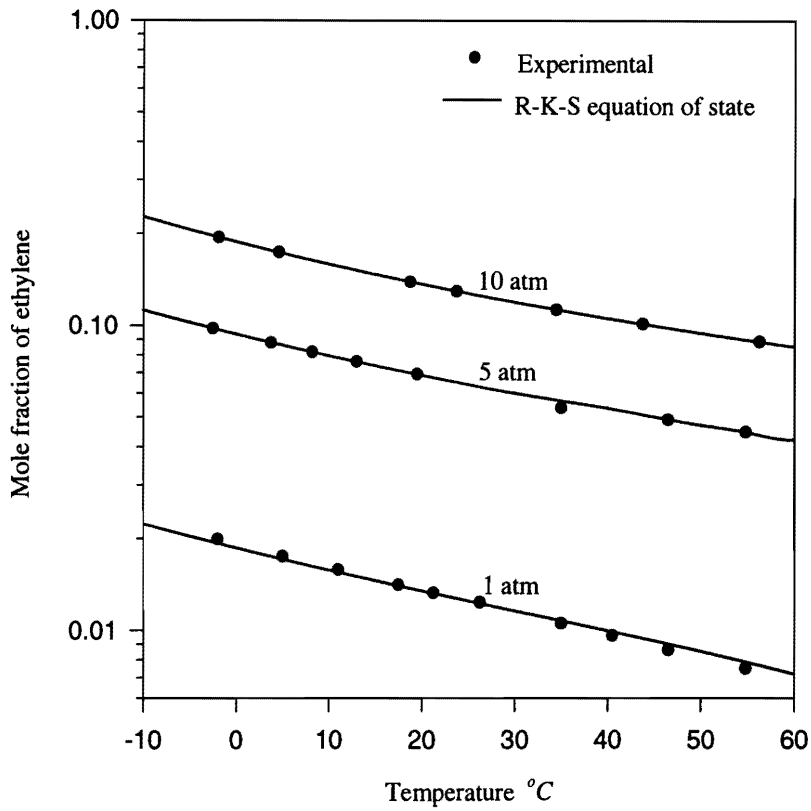

Figure 1. Comparison of the model-predicted solubility of ethylene in toluene at 1, 5, and 10 atm with the experimental values.

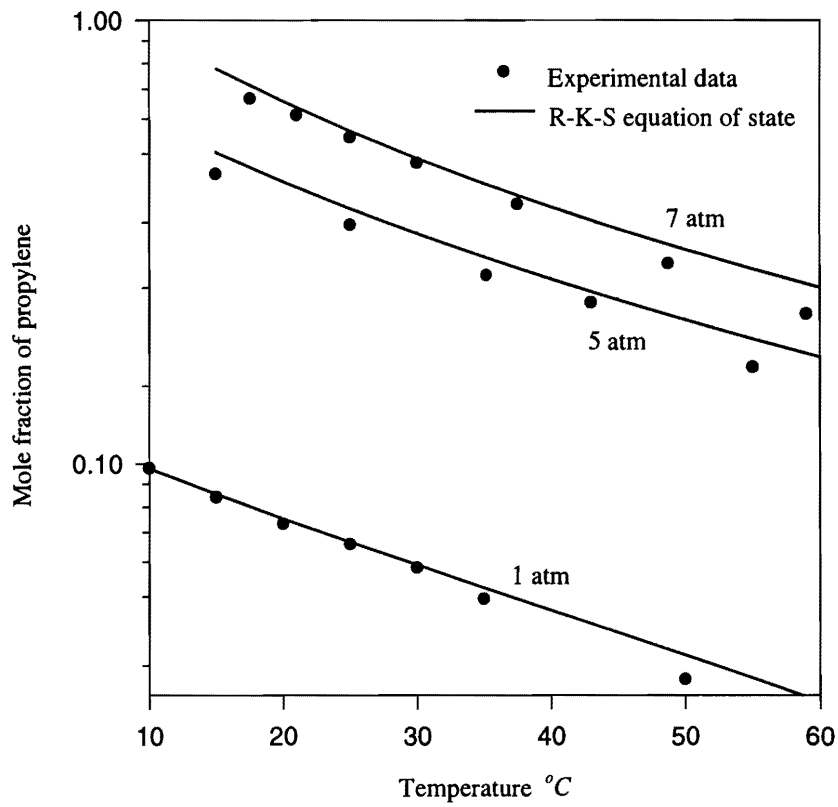

Figure 2. Comparison of the model-predicted solubility of propylene in toluene at 1, 5, and 7 atm with the experimental values.

The run time-dependent average catalytic activity corresponding to 1 hr, that is, $\bar{r}_P$ (60 min) is 6.78×10^4 *kg PE/[(mol Zr) (hr) [C_2H_4]]*. This value, calculated according to Equation 4, is lower than the normalized instantaneous catalytic activity or polymerization rate $\hat{r}_P$ (60 min) = 5.68×10^4 *kg PE/[(mol Zr) (hr) [C_2H_4]]* (see Equation 3). Note that $\bar{r}_P$ (60 min) and $\hat{r}_P$ (60 min) have the same unit. But their physical significance differs. The $\bar{r}_P$ (60 min) should, on principle, agree with the value calculated from the polymer obtained in 1 hr. The above polymerization rate/activity unit follows from the material balance equation and reflects the combined influence of temperature and pressure.

Figure 3 also shows that the kinetic rate profile, which demonstrates the catalytic stability, has an acceleration period of 13 min during which the normalized polymerization rate $\hat{r}_P$ (t) increased till it reached a maximum of 7.60×10^4 *kg PE/[(mol Zr) (hr) [C_2H_4]]*. This maximum value indicates the region of superactivity which signals the thermal and viscosity runaway problems. Following this period, the catalyst started to deactivate.

Under the chosen polymerization conditions, the Cp_2ZrCl_2/MAO catalyst system did not show any induction period. The increase and decrease in $\hat{r}_P$ (t) may be attributed to the formation and destruction of the cationic active zirconium sites, respectively.

Nonisothermal, Uncontrolled Mode of Polymerization

Table 1 summarizes the catalytic activity and the thermal characteristics of the synthesized polymers at two stirring levels. Stirring at 450 and 950 rpm refers to diffusion-controlled and nondiffusion-controlled, external gas–liquid mass transfer resistance-free regimes of mixing, respectively. With respect to the nondiffusion-controlled regime of mixing, the run time-average copolymerization catalytic activity and the peak reaction exotherm increased. At 950 rpm, the copolymerization catalytic activity and the peak reaction exotherm exceeded those in homopolymerization.

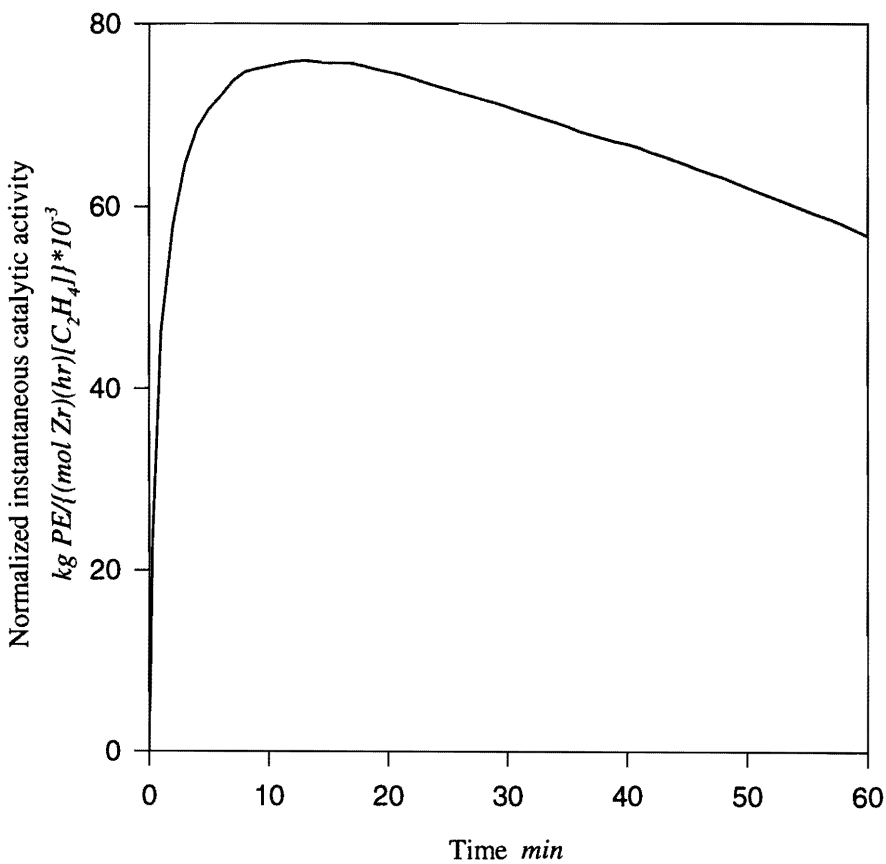

Figure 3. Normalized ethylene polymerization rate as a function of reaction time for the Cp_2ZrCl_2/MAO catalytic system (calculated according to the current engineering approach). Temperature = 50°C, ethylene partial pressure = 10 psi, and Al:Zr = 3,223.

Figure 4 shows that all the polymerization runs proceeded without an induction period. Each reaction exotherm profile was of decay-type. The copolymerization exotherm profile at 450 rpm lies below the homopolymerization exotherm profile at 950 rpm. However, the converse occurs for the copolymerization exotherm profile at 950 rpm.

The reaction exotherm profiles show the catalytic stability, qualitatively approximated by the difference between the maximum and the terminal reaction exotherm values. The greater is the difference, the less stable is the catalyst. Based on this criterion, $Et(Ind)_2ZrCl_2$ shows more stability at 450 rpm than at 950 rpm. Note that the reaction exotherm profiles represent a qualitative equivalence of the polymerization kinetic profiles which also show the catalytic stability. Additionally, the reaction exotherm profiles traced the polymerization history and the associated thermal perturbations.

The following text summarizes the thermal properties of the synthesized polymers. The weight- and number-average solution crystallization temperatures (T_w and T_n) of the copolymers, like the corresponding polymer peak melting temperatures, were below those of the ethylene homopolymers. The effect of side chain branching, that is, incorporation of 1-hexene on the ratio of $T_w:T_n$ revealed as follows: for the homopolymers, $T_w:T_n < 1$ whereas for the copolymers, $T_w:T_n > 1$.

The peak melting temperature and the density of the copolymers were lower than those of the homopolymer. This finding is attributed to the butyl side chain branches that resulted from the incorporation of 1-hexene comonomer.

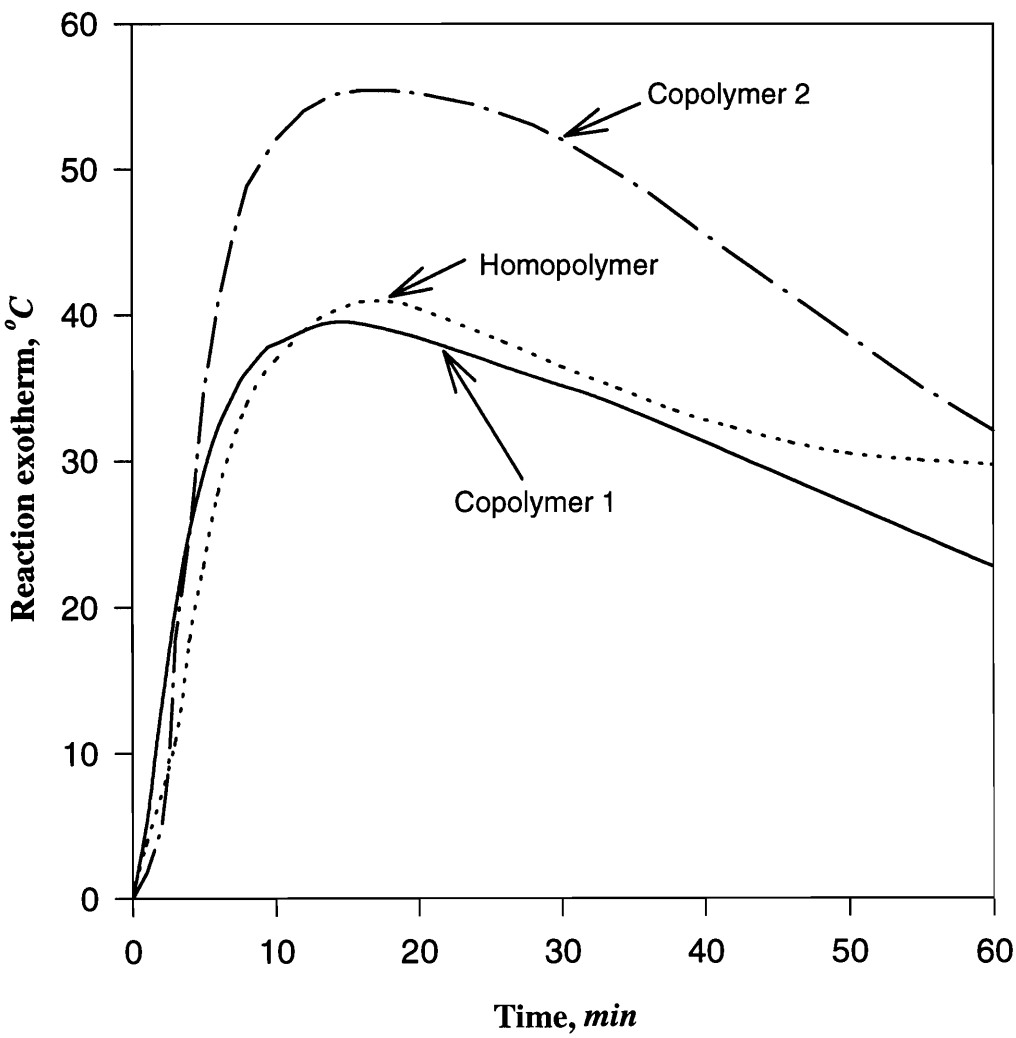

Figure 4. Effect of impeller speed on reaction exotherm profiles. Homopolymer: 950 rpm, Copolymer 1: 450 rpm, and Copolymer 2: 950 rpm.

Table 2 shows how incorporation of 1-hexene affected the microstructure of the synthesized polymers in terms of change in (*a*) molecular weight (polymer backbone length), (*b*) side chain branching (density), and (*c*) soluble fraction. The weight- and number-average molecular weights of the copolymers significantly decreased, irrespective of the variation of the impeller speed. The molecular weight was found to be inversely related to the corresponding run time-dependent average catalyst activity (see Tables 1 and 2). Note that metallocene-catalyzed isothermal polymerization also shows the same inverse relation between molecular weight and activity [1]. Increased chain transfer rate over the propagation rate decreases the molecular weight [33]. The increased chain transfer rate may be attributed to increased β–H elimination rate, 1-hexene acting as a chain transfer agent [34], and σ-bond metathesis competing with the β–H elimination [35].

The polydispersity indices listed in Table 2 illustrate that the nonisothermal operation produced broader molecular weight distribution (MWD) than what an isothermal operation usually does ($2 \leq$ polydispersity index ≤ 3) [1]. Broadening the MWD especially specially to the right indicates the presence of a substantial high molecular weight components. This can affect polymer processability and film optical properties.

Figure 5 compares the differential molecular weight distributions of the experimental polymers. The peak molecular weights and the molecular weight distributions of the resulting copolymers did not significantly vary with the increase of impeller speed from 450 to 950 rpm. This occurred despite variation of the reaction exotherm profiles, that is, polymerization history from one run to other (see Figure 4). However, the peak molecular weight fractions, in each case, slightly decreased with the increase in impeller speed. Copolymerization produced less higher-weight polymer backbones than homopolymerization. This illustrates the chain transfer role played by 1-hexene, even without using hydrogen (the conventional molecular weight regulator).

The overall variation in the polydispersity indices (see Table 2) and the molecular weight distributions (see Figure 5) may be attributed to the varying degrees of the chain termination rate due to β–H elimination, chain transfer by 1-hexene, and the σ-bond metathesis reaction [19].

The side chain branching and crystallinity of the copolymer did not significantly vary with the impeller speed (see Table 2). This shows that mixing conditions did not influence these copolymers properties which reflect the bulk (average) configuration and composition of the resulting copolymer backbones. Note that mixing conditions affect only distributive copolymer properties [3, 5, 6].

$Et(Ind)_2ZrCl_2$ produced more soluble fractions (mainly highly branched and low molecular weight components) at 450 rpm (13.7%) than at 950 rpm (6.6%). This explains the importance of optimizing the mixing condition with respect to polymer properties. The current soluble fraction values are higher than that (~1%) reported for an isothermal metallocene-catalyzed ethylene–1-octene copolymer [36]. The production of the above high soluble fraction is also evident in the corresponding DSC thermogram (see Figure 6). The segregated, bimodal DSC thermogram implies that the resulting copolymer will melt at varying temperatures, causing processing inhomogeniety. This underscores the adverse impact of thermal perturbation in metallocene-catalyzed ethylene–1-hexene copolymerizartion.

Table 2. Microstructural Characteristics of the Synthesized Ethylene Homo- and Copolymers.

Polymerization run number	Chain branching (CH_3 group/ 1000 C)	Crystallinity (%)	Average 1-hexene composition (mole %)	Weight-average molecular weight (g/mol)	Number-average molecular weight (g/mol)	PDI*	Soluble fraction
Homopolymer	Not applicable	80.29	Not applicable	116 994	17 937	6.5	0.0
Copolymer 1	20	36.14	4.3	43 954	11 579	3.8	13.7
Copolymer 2	22	36.66	4.8	46 770	9688	4.8	6.6

*PDI = Polydispersity index.

Figure 6 shows how the mixing level influenced the copolymer composition distribution measured qualitatively by the CRYSTAF technique. An increase in the impeller speed converted a long-tailed, monomodal composition distribution into a segregated, multimodal one (compare curve copolymer 1 with curve copolymer 2 in Figure 6). Better end-uses, especially food packaging, require a minimum level of soluble fractions in the synthesized copolymers. Note that the average copolymer composition, expressed in terms of chain branching and average 1-hexene content (see Table 2), does not reflect these micro-structural composition changes.

The above multimodality physically represents preferential incorporation of 1-hexene in the main polymer chain.

Heterogenized Metallocenes

Table 3 summarizes the binding energy of the Zr 3d spectral lines and the spin–orbit ($3d_{5/2}$–$3d_{3/2}$) splits in the XPS spectra of the catalyst samples as a function of the catalyst preparatory methods. The Zr 3d spectral lines split into Set 1 and Set 2 components. The spin–orbit ($3d_{5/2}$–$3d_{3/2}$) split of Set 1 equals that of Set 2 for each catalyst sample.

The Set 1 Zr $3d_{5/2}$ binding energy of Sample 1 approximates the Zr $3d_{5/2}$ binding energy of 182.7 eV of the silica/Et(Ind)$_2$ZrCl$_2$ reference sample and exceeds the binding energy of Et(Ind)$_2$ZrCl$_2$ by 0.6 eV. This increase in binding energy shows that interaction of Et(Ind)$_2$ZrCl$_2$ with silica makes Zr electron-deficient and produces a zirconocenium cation (Cation 1). The generation of a single cation in the absence of MAO has been, however, observed for thorocene supported on MgCl$_2$ and partially dehydroxylated alumina, using CPMAS NMR [37, 38].

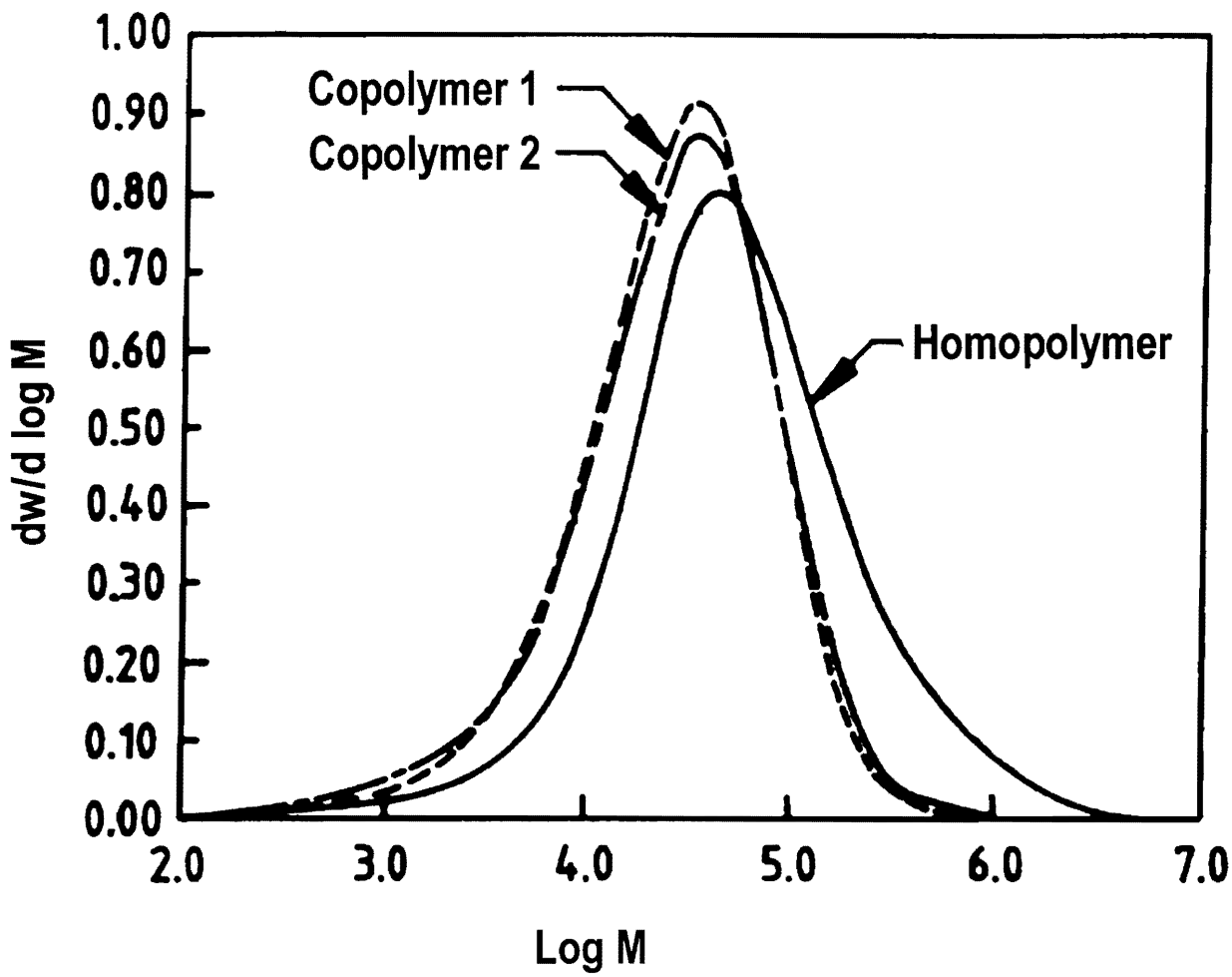

Figure 5. Effect of impeller speed on molecular weight distributions. Homopolymer: 950 rpm, Copolymer 1: 450 rpm, and Copolymer 2: 950 rpm.

The Set 2 Zr $3d_{5/2}$ binding energy of Sample 1 is greater than that of the silica/$Et(Ind)_2ZrCl_2$ reference sample by 0.9 eV. This means that treatment with the MAO cocatalyst makes Cation 1 more electron-deficient, producing a different zirconocenium cation (Cation 2).

The comparison of Set 1 and Set 2 Zr $3d_{5/2}$ binding energies of Samples 2 and 3 with those of the $Et(Ind)_2ZrCl_2$ and silica/$Et(Ind)_2ZrCl_2$ reference samples also support the above findings. Two zirconocenium cations are produced as well in Samples 2 and 3.

Table 3. Zr 3d Binding Energies (eV) and Spin–Orbit ($3d_{5/2}$–$3d_{3/2}$) Split in Set 1 and Set 2 in the XPS Spectra of the Heterogenized $Et(Ind)_2ZrCl_2$.

Sample No.	Catalyst sample description	Peaks of interest	Binding energy (± 0.2 eV)	
1	Silica/$Et(Ind)_2ZrCl_2$/MAO	$Zr3d_{3/2}$	Set 1	184.7
			Set 2	185.7
		$Zr3d_{5/2}$	Set 1	182.6
			Set 2	183.6
		Spin–orbit ($3d_{5/2}$–$3d_{3/2}$) split	Set 1	2.1
		Spin–orbit ($3d_{5/2}$–$3d_{3/2}$) split	Set 2	2.1
2	Silica/MAO/$Et(Ind)_2ZrCl_2$	$Zr3d_{3/2}$	Set 1	185.1
			Set 2	186.1
		$Zr3d_{5/2}$	Set 1	182.8
			Set 2	183.9
		Spin–orbit ($3d_{5/2}$–$3d_{3/2}$) split	Set 1	2.3
		Spin–orbit ($3d_{5/2}$–$3d_{3/2}$) split	Set 2	2.3
3	Silica/MAO-pretreated $Et(Ind)_2ZrCl_2$	$Zr3d_{3/2}$	Set 1	184.9
			Set 2	185.9
		$Zr3d_{5/2}$	Set 1	182.9
			Set 2	183.9
		Spin–orbit ($3d_{5/2}$–$3d_{3/2}$) split	Set 1	2.0
		Spin–orbit ($3d_{5/2}$–$3d_{3/2}$) split	Set 2	2.0
Reference samples				
	$Et(Ind)_2ZrCl_2$	$Zr3d_{5/2}$		182.0
	Silica/$Et(Ind)_2ZrCl_2$	$Zr3d_{5/2}$		182.7

Within the experimental uncertainties, the Set 1 Zr $3d_{5/2}$ binding energies for all the catalyst samples are close to one another. Therefore, Cation 1 resides in a nearly same solid-state electronic environment despite the variation in the heterogenization procedures. The same observation holds for Cation 2 because of the closeness of the Set 2 Zr $3d_{5/2}$ binding energies. However, the electronic environment of Cation 1 differs from that of Cation 2.

The generation of the above zirconocenium cations, one referring to Set 1 and the other to Set 2, appears to fairly support the following postulated surface chemistry (see Scheme 1).

In Method 1, $Et(Ind)_2ZrCl_2$ reacts with the silica surface OH groups first to form presumably in the form of a zirconocenium ion-pair $[SiO]^-[Et(Ind)_2ZrCl]^+$ (Cation 1) [39, 40]. When it is subsequently treated with MAO, the following occurs. MAO, being a Lewis acid, methylates $Et(Ind)_2ZrCl_2$. Consequently, a bridged zirconocenium methyl species (Cation 2), presumed to be trapped and stabilized in multi-coordinate crown alumoxane complex(es), is produced [41, 42]. These zirconocenium cations provide the polymerization catalytic sites.

In Method 2, MAO first reacts with the silica surface OH groups to form the stable Si–O–Al bonds. The surface-anchored MAO plays the following roles: methylation, Cl^- ion abstraction, and crown alumoxane complex(es) formation (Cation 2) [41–43]. The abstracted Cl^- is also postulated to be trapped and stabilized in multi-coordinate alumoxane complex(es) [41, 42].

In Method 3, the preactivation of $Et(Ind)_2ZrCl_2$ by MAO in solution first forms, through the same mechanism as referred to in Method 2, the crown alumoxane complex(es) [44] (Cation 2), which next anchor(s) with the silica surface OH groups.

Chen *et al.* [39] postulated that in Method 1 (Sample 1), treatment with MAO generates an ion pair in the form of $[SiO]^-[Et(Ind)_2ZrCH_3]^+$. The present XPS results refute this postulation by indicating that the resulting zirconocenium cation appears as crown alumoxane complex(es) (Cation 2).

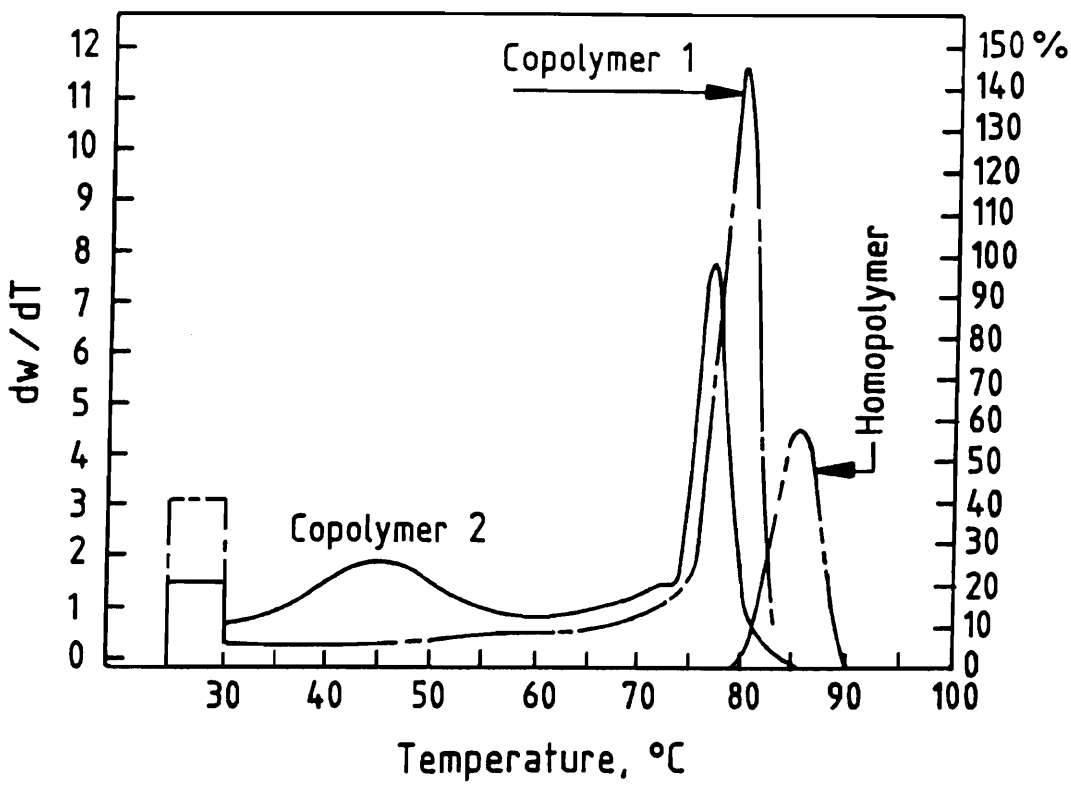

Figure 6. Effect of impeller speed on copolymer composition distribution. Homopolymer: 950 rpm, Copolymer 1: 450 rpm, and Copolymer 2: 950 rpm.

The genesis of Cation 1 in Methods 2 and 3 can be explained as follows. MAO and MAO-pretreated $Et(Ind)_2ZrCl_2$ selectively react in Methods 2 and 3, respectively, with the silica surface OH groups. Consequently, a portion of the total surface OH groups remains unreacted. $Et(Ind)_2ZrCl_2$ reacts with these remaining OH groups to produce Cation 1. In Method 2, a part of the finally added $Et(Ind)_2ZrCl_2$ reacts with the remaining OH groups to produce Cation 1. However, in Method 3, the $Et(Ind)_2ZrCl_2$ in equilibrium with the MAO-pretreated $Et(Ind)_2ZrCl_2$ solution provides the source for reaction with the OH groups to generate Cation 1.

Note that the current XPS findings partially match what Gassman and his coworkers reported with respect to MAO-preactivated zirconocenes dissolved in toluene solution [45, 46]. The overall conclusion is that the generation of the metallocenium cation is a common phenomenon in the solution and solid state.

Figure 7 shows a typical micro-PIXE energy spectrum from one of the catalyst samples. This evidences the several trace element impurities such as K, Ca, Ti, Fe, Ni, Cu, and Zn which may potentially poison the resulting catalyst.

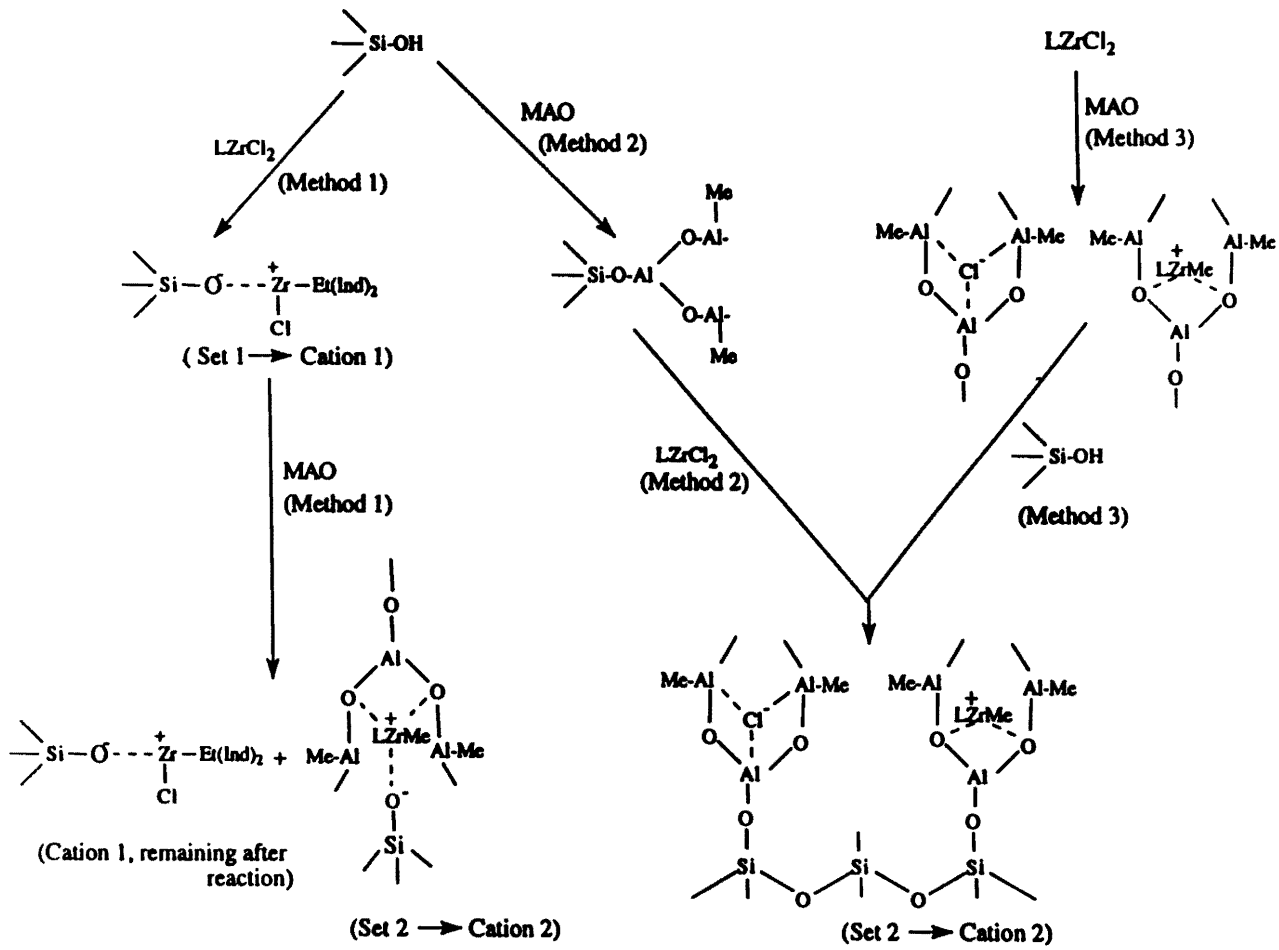

where MAO = -O-Al(Me)-O-Al(Me)-O-Al(Me)-, Me = CH_3, L = $Et(Ind)_2$; the generation of Cation 1 in Methods 2 and 3 is explained in the text.

Scheme 1. Surface chemistry related to the formation of the zirconocenium cations in the heterogenized catalyst samples [39–44].

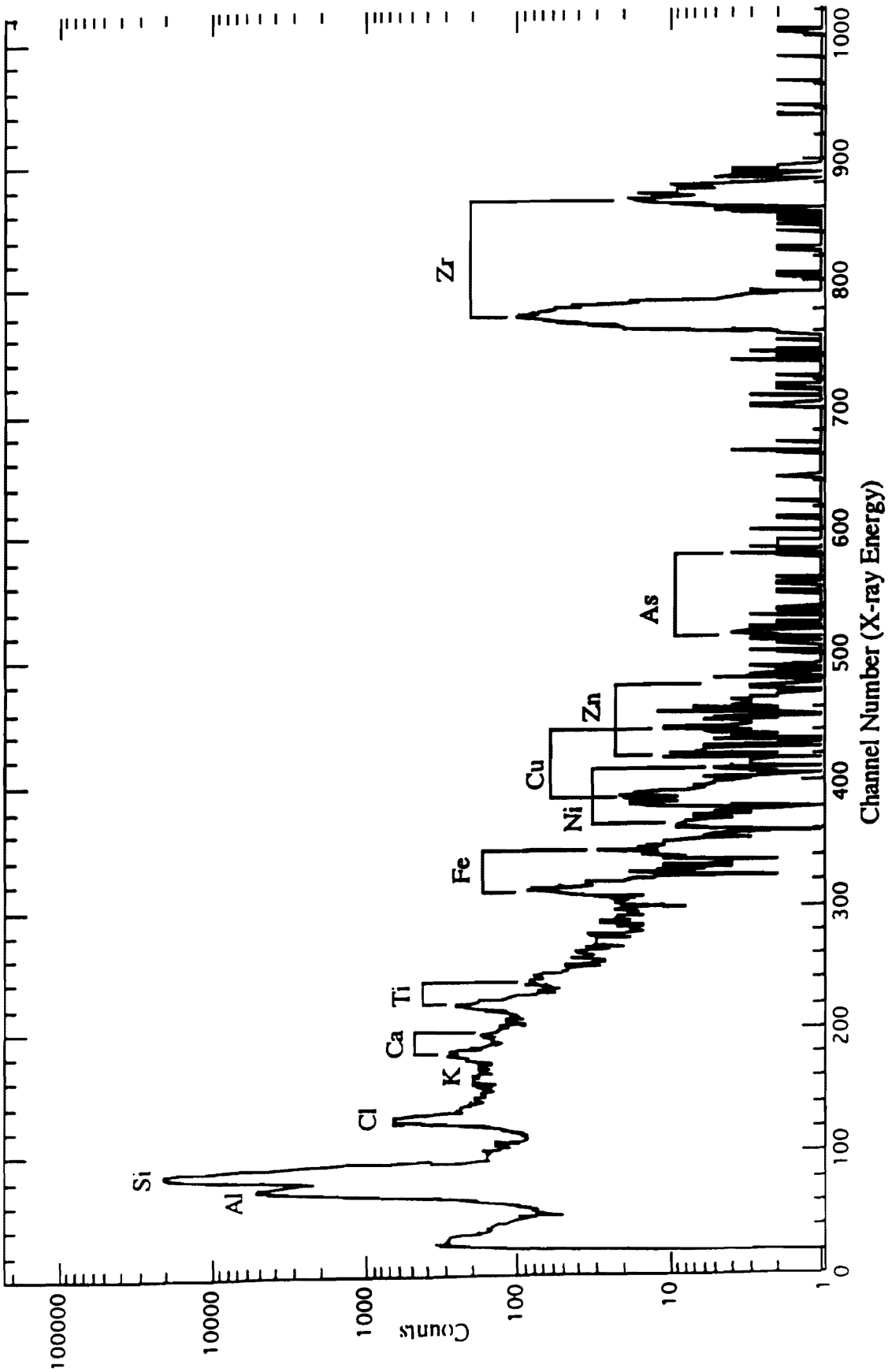

Figure 7. A typical micro-PIXE energy spectrum of the heterogenized catalyst sample. All the samples evidence the detected impurities.

5. CONCLUSIONS

Based on the present work, we conclude the following:

- The solubility prediction model matches the experiment. Therefore, the output of this model can be incorporated into the present engineering approach to advantageously show the combined influence of temperature and pressure on the polymerization rate, the catalytic activity, and the stability profile.
- For evaluating the performance of a catalyst system, the catalytic stability profile (which patents have generally ignored), induction period, maximum and terminal polymerization rates ($\hat{r}_{P,\max}$ and $\hat{r}_P(t_R)$), and run time-dependent average polymerization activity $\bar{r}_P(t_R)$ must be reported.
- Non-isothermal, uncontrolled polymerization conducted in varying mixing regimes can illustrate the influence of mixing, reaction exotherm, and thermal perturbations on the structural stability of the experimental metallocene, the catalytic activity, polymerization performance, and the properties of the resulting polymers. Thermal perturbations broadened the polydispersity index.
- With the change in level of stirring from diffusion-controlled regime to nondiffusion-controlled, external gas–liquid mass transfer resistance-free one, a segregated, multimodal copolymer composition distribution was obtained.
- Mixing significantly affected only the copolymer composition distribution and soluble fraction but not the bulk polymer properties.
- Incorporation of 1-hexene significantly decreased the production of high molecular weight fractions without using hydrogen (the conventional molecular weight regulator), the average molecular weights and density but increased the run-time dependent average catalyst activity, the peak melting temperatures and the weight- and number average solution crystallization temperatures.
- Heterogenization of $Et(Ind)_2ZrCl_2$ and MAO generated two types of zirconocenium cations (Cation 1 and Cation 2), independent of the heterogenization methods. Based on the postulated surface chemistry, Cation 1 is presumed to be in the form of an ion-pair $[SiO]^-[Et(Ind)_2ZrCl]^+$ while Cation 2, a trapped multi-coordinated crown complex of MAO. In absence of MAO, only Cation 1 is formed. The present study provides some support to the postulated surface chemistry regarding heterogenization of $Et(Ind)_2ZrCl_2$ and MAO on silica.
- Trace element impurities such as K, Ca, Ti, Fe, Ni, Cu, and Zn may be the potential source of catalyst poisoning.

ACKNOWLEDGMENTS

The authors acknowledge the support provided by the Research Institute and the Physics Department of the King Fahd University of Petroleum & Minerals (KFUPM) at Dhahran, Saudi Arabia for the present study. The industrial collaboration and fund provided by SABIC R&D are especially acknowledged. The technical assistance of Messrs. Khurshid Alam and Munawwar Khan is appreciated. The authors also thank Dr. Benjamin Monrabal of PolyChar at Spain for the Crystaf analysis. The molecular weight characterization done by Polymer Laboratories, UK, using GPC 210, and the donation of 1-hexene by Chevron, Switzerland are highly acknowledged.

REFERENCES

[1] The Research Institute, *Development of Heterogeneous Metallocene Catalysts for Olefin Polymerization. Phase I: Comprehensive Literature Review.* King Fahd University of Petroleum and Minerals, Dhahran, Saudi Arabia, 1996, p. 295.

[2] P.M. Morse, *Chem. and Eng. News*, July 6, 1998, p. 11.

[3] M. Atiqullah and E.B. Nauman, *Chem. Eng. Sci.*, **45** (1990), p. 1267.

[4] G. Tosun, *AICHE J.*, **38(3)** (1992), p. 425.

[5] M. Atiqullah, *Eur. Polym. J.*, **29** (1993), p.1581.

[6] M. Atiqullah, M.M. Hassan, and S.A. Beg, *J. Appl. Polym. Sci.*, **46** (1992), p. 879.

[7] L.L. Böhm, *Polymer.*, **19** (1978), p. 553.

[8] I. Kim, J.H. Kim, and S.I. Woo, *J. Appl. Polym. Sci.*, **39** (1990), p. 837.

[9] J.H. Kim, I. Kim, and S.I. Woo, *Ind. Engg. Chem. Res.*, **30** (1991), p. 2074.

[10] I. Kim, H.K. Choi, J.H. Kim, and S.I. Woo, *J. Appl. Polym. Sci.*, **52** (1994) p. 1739.

[11] S.M. Walas, *Phase Equilibria in Chemical Engineering*. Stoneham: Butterworth, 1985, p. 139.

[12] T.E. Daubert, *Chemical Engineering Thermodynamics*. New York: McGraw-Hill, Inc., 1985, p. 294.

[13] J.M. Prausnitz, R.N. Lichtenthaler, and E.G. de Azevedo, *Molecular Thermodynamics of Fluid Phase Equilibria*. Englewood Cliffs, New Jersey: Prentice-Hall, Inc., 1986, p. 465.

[14] S.I. Sandler, *Chemical and Engineering Thermodynamics*. New York: John Wiley & Sons, Inc., 1989, p. 146.

[15] G. Soave, *Chem. Eng. Sci.*, **27** (1972), p. 1197.

[16] W. Gellert, S. Gottwlad, M. Hellwich, H. Kästner, and H. Hüstner (eds.), *The VNR Concise Encyclopedia of Mathematics*. New York: Van Nostrand Reinhold, 1989, p. 99.

[17] M. Atiqullah, H. Hammawa, and H. Hamid, *Proc. 4th International Congress on Metallocene Polymers: Metallocene ASIA 1997*, 1997, p. 227.

[18] M. Atiqullah, H. Hammawa, and H. Hamid, *Eur. Polym. J.*, **34(10)** (1998), p. 1581.

[19] M. Atiqullah, H. Hammawa, M.N. Akhtar, J.H. Khan, and H. Hamid, *J. Appl. Polym. Sci.*, **70** (1998), p. 137.

[20] M. Atiqullah, M. Faiz, M.N. Akhtar, M.A. Salim, S. Ahmed, and J.H. Khan, *Surf. and Interf. Anal.* (in press).

[21] D.Briggs and M.P. Seah, *Practical Surface Analysis, 2nd edn.* New York: John Wiley, 1990, p. 542.

[22] M. Ahmed, J. Nickel, A. Hallak, R. Abdel-Aal, A. Coban, H. Al-Juwair, and M. Aldaous, *Nucl. Instr. and Meth.*, **B82** (1993), p. 584.

[23] M. Atiqullah, A. Ahmed, M.N. Akhtar, S. Ahmed, and J.H. Khan, *J. Radio Anal. and Nuclear Chem*, 1998 (in press).

[24] Y. Perrin, R. Bangnara, T. Berners-Lee, W. Caren, R. Divia, C. Parkman, J. Peterson, L. Tremblet, and B. Wessels, *The VALET-plus Embeded in Large Physics Experiments*. Geneva: Data Handling Division, CERN, 1988.

[25] *Kmax: An Advanced CAMAC Data Acquisition and Control Environment for Real Time Interaction and Event-by-Event Data with Sorting, Histograming and Data Analysis*. Sparrow Inc., USA, 1989.

[26] J.A. Maxwell, J.L. Campbell, and W.J. Teesdale, *Nucl. Instr. Meth.*, **43** (1988), p. 218.

[27] J.M. Prausnitz, R.N. Lichtenthaler, and E.G. Azevedo, *Molecular Thermodynamics of Fluid Phase Equilibria*. Englewood Cliffs, NJ. Prentice-Hall: 1986, p. 465.

[28] S.I. Sandler, *Chemical and Engineering Thermodynamics*. New York: John Wiley and Sons, 1989, pp 146–149.

[29] L.L. Bohm, *Polymer*, **19** (1978), p.553.

[30] M.D. Donohue and J.M. Prausnitz, *A.I. Ch. E. J.*, **24** (1978), p. 849.

[31] Y. Song, S.M. Lambert, and J.M. Prausnitz, *Ind. Eng. Chem. Res.*, **33** (1994), p. 1047.

[32] J.M.V. Estrada and A.E. Hamielec, *Polym.*, **35** (1994), p. 808.

[33] I. Lee, W.J. Gauthier, J.M. Ball, B. Iyengar, and S. Collins, *Organometallics*, **11** (1992), p. 2115.

[34] J. Seppälä, *J. Appl. Polym. Sci.*, **30** (1985), p. 3545.

[35] J.C.W. Chien and D. He, *J. Polym. Sci.: Part A: Polym. Chem.*, **29** (1991), p. 1585.

[36] T. Uozumi and K. Soga, *Makromol Chem.*, **193** (1992), p. 828.

[37] P.J. Toscano and T.J. Marks, *J. Am. Chem. Soc.*, **107** (1985), p. 653.

[38] D. Heddon and T.J. Marks, *J. Am. Chem. Soc.*, **110** (1988), p. 1647.

[39] Y-X. Chen, M.D. Rausch, and J.C. Chien, *J. Polym. Sci.: A: Polym. Chem.*, **33** (1995), p. 2093.

[40] W. Kaminsky, F. Renner, and H. Winkelbach, *Worldwide Metallocene Conference, Metcon 94, Houston, Texas, U.S.A.*, May 25–27, 1994, p. 11.

[41] K. Soga and M. Kaminaka, *Macromol. Chem. and Phys.*, **195** (1994), p. 1369.

[42] J.C.W. Chien and D. He, *J. Polym. Sci.: A: Polym. Chem.*, **29** (1991), p. 1603.

[43] F. Ciardelli, A. Altomare, and M. Michelotti, *Cat. Today*, **41** (1998), p. 149.

[44] C.J. Harlon, S.G. Bott, and A.R. Barron, *J. Am. Chem. Soc.*, **117** (1995), p. 6465.

[45] P.G. Gassman and M.R. Callstrom, *J. Am. Chem. Soc.*, **109** (1987), p. 7875.

[46] P.G. Gassman, D.W. Macomber, and S.M. Willging, *J. Am. Chem. Soc.*, **107** (1985), p. 2380.

Paper Received 28 November 1998; Revised 25 April 1999; Accepted 23 May 1999.